Anisotropic Franck-Condon factors in suspended carbon nanotube quantum dots

Fabio Cavaliere[1], Eros Mariani[2], Renaud Leturcq[3,4], Christoph Stampfer[3,5] and Maura Sassetti[1]
[1] *LAMIA CNR, Dipartimento di Fisica, Università di Genova, Via Dodecaneso 33, 16146 Genova, Italy*
[2] *Institut für Theoretische Physik, Freie Universität Berlin, Arnimallee 14, 14195 Berlin, Germany*
[3] *Laboratory for Solid State Physics, ETH Zurich, 8093 Zurich, Switzerland*
[4] *IEMN CNRS-UMR 8520, ISEN, Avenue Poincaré, BP 60069, 59652 Villeneuve d'Ascq Cedex, France*
[5] *JARA-FIT and II. Institute of Physics, RWTH Aachen University, 52074 Aachen, Germany*
(Dated: November 11, 2009)

Electronic states and vibrons in suspended carbon nanotube quantum dots have in general different location and size. As a consequence, the conventional Anderson-Holstein model, usually employed to study transport properties, is no longer justified. In this paper a more refined model is proposed, which exhibits space-dependent Franck-Condon factors, responsible of important effects detected in the transport spectra. Our model is consistent with recent measurements and its predictions can be relevant for tunneling experiments in nano-electromechanical systems.

PACS numbers: 73.23.-b; 85.85.+j; 78.32.-k

Introduction — Advances in miniaturization have paved the way to the fabrication of nanodevices in which molecular systems become active elements of circuits [1]. Transport-induced tunneling of electrons through molecules leads to the excitation/de-excitation of quantized vibrational modes (vibrons) which have been experimentally observed in fullerenes [2] and in suspended carbon nanotubes (CNT) [3, 4, 5, 6]. The latter are particularly interesting due to their remarkable electronic properties and the rich physics of their vibrons. Indeed, radial breathing modes [3] as well as stretching ones [4, 5] have been probed in recent transport experiments.

Most theoretical studies of transport in suspended CNT quantum dots [7, 8] rely on the Anderson-Holstein (AH) model in which the total charge of the dot is coupled to the vibron displacement. The coupling constants have been analyzed microscopically [9, 10, 11] and result in position-independent Franck-Condon (FC) factors [12] which crucially affect the tunneling transport properties [13, 14, 15]. The predicted low bias suppression of current and the intensity of the vibrational sidebands have been confirmed in a recent experiment [5].

The size and location of the dot and of the vibron are generally not directly related to each other, as the mechanisms generating them are physically distinct. In this paper we focus on the theoretical analysis of this scenario, discussing a model in which electronic tunneling in the CNT yields *position-dependent* FC factors, revealing striking effects beyond the conventional AH treatment. Indeed, as the mechanical deformations couple to the local electronic density, the FC suppression of tunneling is stronger in the vicinity of the vibron. In order to deduce this picture microscopically, we discuss the coupling of the vibron to the electronic zero modes as well as to plasmonic excitations of the dot. Our analysis shows that transport yields strongly anisotropic features when the dot size L_d is *larger* than the vibron length L_v and the latter locates close to one edge.

Our predictions find a nice confirmation in further measurements on the same experimental setup already considered in Ref. 5. Here a quantum dot is formed below a top gate in the central region of a suspended CNT. A scanning electron microscope image of the device is shown in Fig. 1a. The suspended CNT is electrically and mechanically connected to both source (S) and drain (D) contacts, while a central suspended electrode (TG) is not electrically connected, and acts as a middle suspended top-gate. A quantum dot in the CNT is formed between defects along the nanotubes, which are presumably created during the release process and act as local barriers (more details are given in Ref. 5). The configuration of double top- and back-gates allow to extract the approximate position of the quantum dot, which is located below the TG in the central region of the sus-

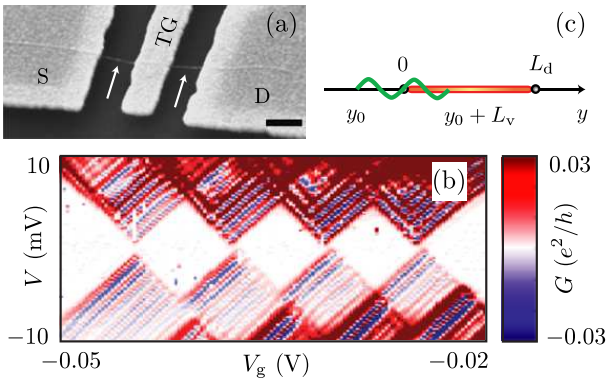

FIG. 1: (a) Scanning electron microscope of the suspended carbon nanotube (arrows denote its position) connected to source (S) and drain (D) contacts. A top gate (TG) is also present. Scale bar: 200 nm. (b) Experimentally determined differential conductance G as a function of the top gate voltage V_g and bias V. (c) Schematic view of the coupled quantum dot-vibron system. The thick part represents the spatial extent of the quantum dot and the wiggly line the vibron.

pended CNT, and its electronic size ($L_{\rm d} \approx 240$ nm) is determined from Coulomb diamond measurements. Electronic transport measurements have been carried-out in a pumped ^{4}He cryostat with a standard lock-in technique. A typical spectrum of the differential conductance G is shown in Fig. 1b. It exhibits an almost perfect four-fold degeneracy of the Coulomb blockade diamonds (due to the valley and spin degeneracy of electrons in CNT) and a rich structure of sidebands due to the excitation of stretching vibrons ($L_{\rm v} \approx 60$ nm). The relevant features to be stressed are: *i*) the strong suppression of vibrational sidebands with negative slopes; *ii*) the alternating pattern of positive and negative differential conductance (PDC/NDC) traces with a positive slope; *iii*) the asymmetric intensity of G for positive/negative bias. A simple asymmetry (no matter how large) in the tunneling transparency of the lead-dot barriers cannot account for the complete suppression of sidebands with one slope, as exemplified in Fig. 3b later and in the related analysis. The direct comparison of our model with experiments suggests the importance of anisotropic FC factors and allows to estimate the minimum quality factor of the CNT needed to observe the NDC pattern.

Anisotropic coupling — To elucidate the mechanism leading to anisotropic FC factors we start with a single electronic state coupled to the lowest vibrational stretching mode. The dot is confined between $y_1 = 0$ and $y_2 = L_{\rm d}$ and the vibron is clamped at y_0 and $y_0 + L_{\rm v}$, with $-L_{\rm v} < y_0 < L_{\rm d}$ for a finite overlap between the two systems (see Fig. 1c). We treat the dot Hamiltonian as a Luttinger liquid with open boundaries [16] (i.e. the electronic field fulfills $\psi(0) = \psi(L_{\rm d}) = 0$) with $H_{\rm d} = E_{\rm c}N^2 + 2^{-1}\sum_{q=1}^{\infty}\left[p_q^2 + \omega_q^2 x_q^2\right] = H_{\rm d}^{(\rm N)} + H_{\rm d}^{(\rm pl)}$. Here, N is the dot excess charge zero mode, $E_{\rm c}$ the charging energy and x_q, p_q the generalized position and momentum of the q-th plasmon mode with frequency $\omega_q = \pi v_{\rm c} q/L_{\rm d}$ and group velocity v_c [17]. In complete analogy, the lowest stretching mode is described by the harmonic Hamiltonian $H_{\rm v} = p_0^2/2M + M\omega_0^2 x_0^2/2$, where M is the vibron mass, $\omega_0 = \pi v_{\rm s}/L_{\rm v}$ its frequency and $v_{\rm s}$ the stretching mode velocity [17]. The coordinate x_0 represents the amplitude of the lowest vibron, described by the distortion field $u(y) = \sqrt{2}x_0 \sin\left[\pi(y-y_0)/L_{\rm v}\right]$, and p_0 is the conjugate momentum. In a CNT, $v_{\rm s} < v_{\rm c}$, and the above experimental estimates yield $\omega_0 < \omega_1$ [4, 5]. Electrons and vibrations are microscopically coupled via

$$H_{\rm d-v} = c\int_{\max[0,y_0]}^{\min[L_{\rm d},y_0+L_{\rm v}]} {\rm d}y\,[\rho_{\rm R}(y)+\rho_{\rm R}(-y)]\partial_y u(y) \quad (1)$$

where c is the deformation potential coupling constant [17, 18, 19] and $\rho_{\rm R}(y) = (N/2L_{\rm d}) + (1/2\pi)\partial_y\phi(y)$ is the right movers electron density with $\phi(y) = \sqrt{\omega_1/2}\sum_{q>0} e^{-\xi\pi q/2L_{\rm d}}[e^{-i\pi qy/L_{\rm d}}(x_q - i\omega_q^{-1}p_q) + {\rm h.c.}]$ the plasmon field ($\hbar = 1$, ξ is the short wavelength cutoff). This expression of the density neglects the fast oscillating terms due to mixed right and left-moving fermion fields and is reliable in the large N regime with $N \gg L_{\rm d}/\pi L_{\rm v}$.

The coupling Eq. (1) can be decomposed into $H_{\rm d-v}^{(\rm N)} = c_0 x_0 N$ and $H_{\rm d-v}^{(\rm pl)} = x_0\sqrt{M}\sum_{q=1}^{\infty} c_q x_q$, respectively due to zero modes and plasmons. Here we have introduced the coupling terms

$$c_0 = \frac{\omega_0^{\frac{3}{2}}\sqrt{M}\delta}{\pi}\lambda_{\rm m}\sin(\pi\Delta)\theta(\Delta)\theta(1-\Delta) \quad (2)$$

$$c_q = \frac{\omega_0^{\frac{3}{2}}\sqrt{2\omega_1}\lambda_{\rm m} q\delta}{\pi(1-q^2\delta^2)}\{\sin[\pi\delta(\Delta-1)] + q\delta\sin(\pi q\delta\Delta)\} \quad (3)$$

with $\Delta = 1 + y_0/L_{\rm v}$, $\delta = L_{\rm v}/L_{\rm d}$ and $\lambda_{\rm m} = c/(v_{\rm s}\sqrt{M\omega_0})$ [20]. The total Hamiltonian $H_{\rm dot-vib} = H_{\rm d} + H_{\rm v} + H_{\rm d-v}$ is quadratic in the generalized coordinates and is thus easily diagonalized [14, 21] into (details will be given elsewhere [22])

$$H_{\rm dot-vib} = \sum_{\nu\geq 0}\Omega_\nu a_\nu^\dagger a_\nu + E_c^* N^2\,, \quad (4)$$

where $a_\nu^\dagger$ creates the new modes: those with $\nu \geq 1$ representing dressed plasmons, while $\nu = 0$ describing a vibronic excitation dressed by plasmons. Their energies are given by the solutions of $\Omega_\nu^2 = \omega_0^2 + \sum_{q=1}^{\infty} c_q^2/\left(\Omega_\nu^2 - \omega_q^2\right)$ and always satisfy $\Omega_0 < \omega_0$ and $\Omega_\nu > \omega_\nu$ for $\nu \geq 1$. In Eq. (4) the charging energy $E_c^* = E_c - (c_0/\sqrt{2M})^2\sum_{\nu\geq 0}(k_{0\nu}/\Omega_\nu)^2$ shows a polaronic shift, with $k_{0\nu}^2 = 1 + \sum_{q=1}^{\infty} c_q^2/(\Omega_\nu^2 - \omega_q^2)^2$. The above transformations affect the electronic field as well. Indeed, the bosonization of the right movers gives [16] $\psi_{\rm R}(y) = (2\pi\xi)^{-1/2} e^{-i\vartheta} e^{i\pi yN/L_{\rm d}} e^{i\phi(y)}$ with $[\vartheta, N] = i$. As we analyze electronic tunneling at energies *smaller* than the plasmon excitations we consider the restricted Hilbert space of the $\nu = 0$ normal mode. It is crucial to realize that, due to the electron-vibron coupling Eq. (1), vibron operators appear in the electronic field. The truncated field operator after the transformations above reads [23]

$$\psi_{\rm R}(y) \approx \frac{e^{-i\vartheta}}{\sqrt{2\pi\xi}} e^{-\lambda_0(y)[a_0^\dagger - a_0]} e^{i\lambda_1(y)[a_0^\dagger + a_0]}\,, \quad (5)$$

where one has $k_{00}^{-1}\lambda_j(y) = (1-j)c_0/\sqrt{2M\Omega_0^3} + \sqrt{\omega_1/\Omega_0}\sum_{q\geq 1} c_q(\Omega_0^2 - \omega_q^2)^{-1}\sin(\pi qy/L_{\rm d} + j\pi/2)$.

In order to analyze the implications of this result, we consider the quasiparticle wavefunction $X_{ll'}(y) = 2\pi\xi\left|\langle N-1, l|\psi_{\rm R}(y)|N, l'\rangle\right|^2$ yielding the local FC factors [7, 14] (here quoted for vibron numbers $l \leq l'$)

$$X_{ll'}(y) = e^{-\lambda^2(y)}[\lambda(y)]^{2(l'-l)}\frac{l!}{l'!}[L_l^{l'-l}(\lambda^2(y))]^2 \quad (6)$$

with a *position-dependent* effective coupling $\lambda^2(y) = \lambda_0^2(y) + \lambda_1^2(y)$. Fig. 2a shows $\lambda(y)$ for different y_0 in the experimentally relevant case $\delta < 1$. Clearly, $\lambda(y)$ is largest in the region where the vibron sits. When

$y_0 < 0$ (thick lines) the value of $\lambda(y)$ is increased due to the coupling of vibrations with the dot charge N, while for $0 \le y_0 \le L_\mathrm{d} - L_\mathrm{v}$ (thin lines) only plasmons contribute and $\lambda(y)$ is sizeable *only* in the proximity of the vibron. Therefore, a spatially-resolved electronic injection along the dot would show a tunneling suppression sensitive to the vibron size and location. Transport experiments involve two electronic tunneling events (on and off the dot) at $y_1 = 0$ and $y_2 = L_\mathrm{d}$. For $y_0 \ge 0$ and a vibron located near one of the tunneling barriers, a strong asymmetry between the values of $\lambda(y)$ at the two tunneling points may occur, in contrast to the more homogeneous case $y_0 < 0$, as shown in Fig. 2b. For $\delta = 1$,

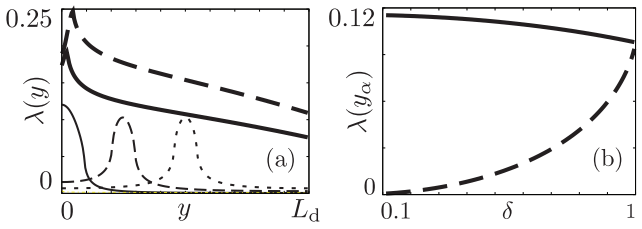

FIG. 2: (a) Plot of $\lambda(y)$ for $\delta = L_\mathrm{v}/L_\mathrm{d} = 0.1$ and different positions of the vibron center $y_\mathrm{c} = y_0 + L_\mathrm{v}/2$: (thick solid) $y_\mathrm{c} = -L_\mathrm{v}/4$; (thick dashed) $y_\mathrm{c} = 0$; (thin solid) $y_\mathrm{c} = L_\mathrm{v}/2$; (thin dashed) $y_\mathrm{c} = L_\mathrm{d}/4$; (thin dotted) $y_\mathrm{c} = L_\mathrm{d}/2$. (b) Plot of $\lambda(y_\alpha)$ vs. δ ($\alpha = 1, 2$) for $y_0 = 0$ and $\alpha = 1$ (solid) ; $\alpha = 2$ (dashed). Notice the strong asymmetry for $\delta \ll 1$ and the symmetric λ's for $\delta = 1$. Here, $v_\mathrm{c}/v_\mathrm{s} = 32$ and $\lambda_\mathrm{m} = 3$ (for a CNT waist $\simeq 1$ nm) [17].

the FC factors are equal and the results are consistent with those of the standard AH model. For $\delta < 1$, only plasmons contribute and the effective couplings become strongly barrier-dependent with an increasing difference when $\delta \to 0$. In this regime, relevant for the experiment, the vibron is located around the left barrier and vibrational excitations are strongly suppressed for tunneling on the right. We also analyzed (not shown) the regime $\delta > 1$ with the vibrating part larger than the dot. Here the asymmetry is lost, the curve is dominated by the zero mode contribution, and we recover the results in [11].

The maximum value of the coupling $\lambda \approx 0.24$ in the regime $\delta < 1$ is crucially sensitive to the ratio $v_\mathrm{s}/v_\mathrm{c}$ and the value of λ_m. The coupling of the dot to the breathing mode reduces the charge velocity [9, 24], increasing $v_\mathrm{s}/v_\mathrm{c}$ towards the WB singularity and allowing to reach $\lambda(y_1) > 1$ with $\lambda(y_2) \ll 1$. Recent measurements in graphene [25] observed a deformation potential larger than expected, which would further increase λ_m.

Transport properties — The model above can be extended to the case of a CNT with two valleys $\eta = \pm 1$ and two spin channels $\sigma = \pm 1$, with $N_{\eta\sigma}$ the number of excess electrons per channel. It is convenient to introduce total (+) and relative (-) charge (c) and spin (s) numbers [26], $N_{c+} = \sum_{\eta\sigma} N_{\eta\sigma}$, $N_{c-} = \sum_{\eta\sigma} \eta N_{\eta\sigma}$, $N_{s+} = \sum_{\eta\sigma} \sigma N_{\eta\sigma}$ and $N_{s-} = \sum_{\eta\sigma} \eta\sigma N_{\eta\sigma}$. Since vibrations couple only to the $c+$ mode [9, 24], the diagonalization of the electron-vibron interaction is equivalent to the one described above. Neglecting high energy plasmons, the Hamiltonian is $H_0 + H_\mathrm{shift} + H_\mathrm{t}$ with

$$
\begin{aligned}
H_0 &= \frac{E_\mathrm{c}}{8}(N_{c+} - N_\mathrm{g})^2 + \frac{\pi v_\mathrm{F}}{8L_\mathrm{d}}\left[N_{c-}^2 + N_{s+}^2 + N_{s-}^2\right] + l\Omega_0\,, \\
H_\mathrm{shift} &= \frac{\Delta\varepsilon}{2}(N_{c+} - N_{c-})\,, \qquad (7) \\
H_\mathrm{t} &= \sum_{\alpha=1,2}\sum_{\eta,\sigma} t_{\alpha,\eta}\psi^\dagger_{\mathrm{R},\eta,\sigma}(y_\alpha)\Psi_{\mathrm{R},\eta,\sigma}(y_\alpha) + \mathrm{h.c.}\,,
\end{aligned}
$$

where $N_\mathrm{g} \propto V_\mathrm{g}$ is the number of charges induced by the gate voltage and $l = a_0^\dagger a_0$. In the dot-vibron Hamiltonian H_0, E_c is the charging term renormalized by the polaronic shift, while H_shift models a shift between the energy of the two valleys $\eta = \pm 1$ [27]. The field $\psi_{\mathrm{R},\eta,\sigma}(y)$ in the tunneling Hamiltonian H_t is the extension of Eq. (5) to the four-channel model and $\Psi_{\mathrm{R},\eta,\sigma}(y_\alpha)$ is the right movers operator for lead α. In sequential tunneling, transition rates are evaluated between eigenstates of H_0. For tunneling *into* the state η of the dot on the barrier α one has [15, 33]

$$
\Gamma^{(\mathrm{in})}_{\alpha,\eta} = \Gamma_0 \frac{|t_{\alpha,\eta}|^2}{|t_{2,+1}|^2} X_{ll'}(y_\alpha) f(\Delta E + (-1)^{\alpha+1} eV/2)
$$

where $\Gamma_0 = 2\pi\mathcal{D}|t_{2,+1}|^2/\xi^2$ and $\mathcal{D}$ is the leads density of states, while $f(E)$ is the Fermi function with ΔE the energy difference between final and initial dot states. Similar expressions hold for tunnel-out processes. Sequential tunneling is justified at high-temperatures $k_\mathrm{B}T > \Gamma_0$ and we further focus on the experimentally relevant regime $\Omega_0 \gg \Gamma_0$, where transport can be described via a rate equation [15, 28, 29] neglecting vibronic coherences. In order to explore the crossover from unequilibrated to equilibrated vibrons, we also introduce a *vibron relaxation* rate [33] $\Gamma^\mathrm{rel}_{l\to l-1} = \exp(\beta\Omega_0)\Gamma^\mathrm{rel}_{l-1\to l} = wl\Gamma_0[1 - \exp(-\beta\Omega_0)]$ from which one obtains the oscillator quality factor $\mathcal{Q} \approx (\Omega_0/\Gamma_0)w^{-1}$ for $k_\mathrm{B}T \ll \Omega_0$ [30], relative to the external dissipative bath. In full generality we consider different regimes, from $\mathcal{Q} = \infty$ to $\mathcal{Q} = 0$ and we also analyze possible asymmetries of left/right tunnel barriers $A = |t_{1,\eta}|^2/|t_{2,\eta}|^2$ and of the coupling between leads and the two valleys $\gamma = |t_{\alpha,-1}|^2/|t_{\alpha,+1}|^2$. The whole phase diagram is extremely rich and will be discussed in detail elsewhere [22]. However, we found that *only one possible parameter range* (discussed below) *is compatible with experimental data* as shown in Fig. 1b: namely, $A < 1$, $\gamma > 1$, $\Delta\varepsilon > 0$ and $\lambda(y_2) \ll \lambda(y_1)$. Fig. 3 shows the differential conductance for non degenerate orbital levels $\Delta\varepsilon > 0$ with isotropic/anisotropic FC factors and with equilibrated/non-equilibrated vibrons. The comparison between Fig. 3a and Fig. 3b clearly shows how a simple (though strong) asymmetry A in the transparency of the left/right barriers within the usual AH

model (Fig. 3b) cannot justify the suppression of sidebands with one slope. The latter is achieved with asymmetric FC factors ($\lambda(y_2) \ll \lambda(y_1)$), see Fig. 3a.

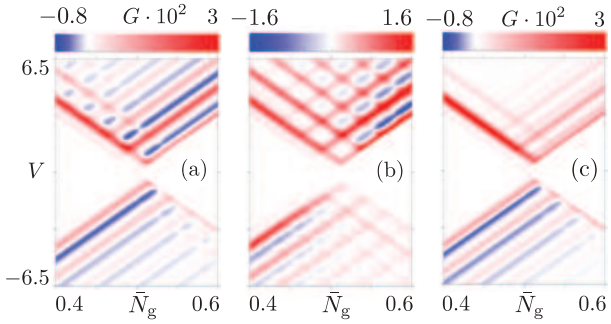

FIG. 3: Plots of the numerical differential conductance G (units e^2/h) as a function of $\bar{N}_g = N_g - 3\pi v_F/2E_c L_d$ and V (units meV). (a) Density plot for $A = 1/20$, $\gamma = 20$, $\lambda^2(y_1) = 2.4$, $\lambda^2(y_2) = 0.1$ for non-equilibrated vibron, $\mathcal{Q} = \infty$; (b) same as in (a) but for $\lambda^2(y_1) = \lambda^2(y_2) = 2.4$; (c) same as in (a) for *equilibrated* vibron, $\mathcal{Q} = 0$. In all panels, $\Omega_0 = 0.8$ meV, $k_B T = 0.08\ \Omega_0$, $E_c = 16$ meV, $\Delta\varepsilon = 0.48$ meV and $\Gamma_0 = 0.8\ \mu$eV. For simplicity, only one resonance is shown.

The origin of the alternating PDC/NDC pattern in our system stems from breaking the valley degeneracy, yielding vibrational sidebands associated to the state $\eta = +1$ interleaved with those of $\eta = -1$. The asymmetry $\gamma > 1$ ($t_{\alpha,+1} < t_{\alpha,-1}$) induces a bottleneck for tunneling events *into* the state $\eta = +1$, leading to a dynamical trap of the empty dot state and a NDC [31, 32]. On the other hand, tunneling into the state $\eta = -1$ provides a fast pathway to enter the dot leading to PDC. The shift $\Delta\varepsilon \neq 0$ creates two different sequences of vibrational sidebands, which repeat the same PDC/NDC pattern as above. Regular alternating PDC/NDC lines cannot be obtained for $\gamma = 1$ and/or degenerate orbital states.
Concerning the role of the left/right asymmetry, one finds that $A < 1$ ($A > 1$) yields NDC lines with the *same* positive (negative) slopes at any voltages. In addition, $A < 1$ allows to obtain a weaker G for $V < 0$ than for $V > 0$. Both features lead to a conductance pattern in close agreement with experiments, see Fig. 1a and Fig. 3a.
We close commenting on the transition from the case of unequilibrated vibrons ($\mathcal{Q} = \infty$, Fig. 3a) to that of fully equilibrated ones ($\mathcal{Q} = 0$, Fig. 3c). As $\mathcal{Q}$ is decreased keeping $A < 1$ and $\gamma > 1$, the NDC pattern for $V > 0$ gradually disappears while the one for $V < 0$ remains almost unaltered and eventually NDC is obtained *only* for $V < 0$. We have numerically investigated the minimum quality factor $\mathcal{Q}_c$ needed to observe at least the first two NDC lines for $V > 0$: for the parameters of Fig. 3 one has $\mathcal{Q}_c \approx 10$, and $\mathcal{Q}_c$ decreases for more asymmetric setups. This value of the Q-factor is compatible with the experimental width of the temperature-broadened anti-Stokes side bands [5].

Conclusions — The study of transport in carbon nanotube quantum dots where vibronic and electronic excitations do not necessarily occupy the same spatial region requires a theory *beyond* the usual Anderson-Holstein model. We show that, when a vibron is embedded into a *larger* dot, *position dependent* Franck-Condon factors arise. The experimentally observed suppression of negative and positive differential conductance lines with negative slopes is interpreted as due to *anisotropic*, barrier-dependent Franck-Condon factors. The experiments seem to indicate that the degeneracy between orbital states of the dot is lifted and that the latter are tunnel-coupled to the leads with different amplitudes. Our predictions can be further checked in spatially-resolved scanning tunnelling microscope measurements.

Acknowledgments — F. C. acknowledges support by INFM-CNR via Seed Project PLASE001. R. L. and C. S. thank K. Inderbitzin, L. Durrer, C. Hierold and K. Ensslin for help and support on the experiment.

[1] A. N. Cleland, Foundations of Nanomechanics (Springer, Berlin, 2003).
[2] H. Park *et al.*, Nature **407**, 57 (2000).
[3] B. J. LeRoy, S. G. Lemay, J. Kong, and C. Dekker, Nature **432**, 371 (2004).
[4] S. Sapmaz *et al.*, Phys. Rev. Lett. **96**, 026801 (2006).
[5] R. Leturcq *et al.*, Nature Phys. **5**, 327 (2009).
[6] A. K. Hüttel *et al.*, Phys. Rev. Lett. **102**, 225501 (2009).
[7] A. Zazunov, D. Feinberg, and T. Martin, Phys. Rev. B **73**, 115405 (2006).
[8] X. Y. Shen, Bing Dong, X. L. Lei, and N. J. M. Horing, Phys. Rev. B **76**, 115308 (2007).
[9] W. Izumida and M. Grifoni, New J. Phys. **7**, 244 (2005).
[10] K. Flensberg, New J. Phys. **10**, 059801 (2008).
[11] E. Mariani and F. von Oppen, Phys. Rev. B **80**, 155411 (2009).
[12] J. Franck, Transactions of the Faraday Society **21**, 536 (1926); E. Condon, Phys. Rev. **28**, 1182 (1926).
[13] S. Braig and K. Flensberg, Phys. Rev. B **68**, 205324 (2003).
[14] A. Mitra, I. Aleiner, and A. J. Millis, Phys. Rev. B **69**, 245302 (2004).
[15] J. Koch and F. von Oppen, Phys. Rev. Lett **94**, 206804 (2005).
[16] M. Fabrizio and A. Gogolin, Phys. Rev. B **51**, 17827 (1995).
[17] Typical CNT parameters: $c \approx 30$ eV, $v_s \approx 2.4 \cdot 10^4$ m/s, $v_F = 8 \cdot 10^5$ m/s and $\rho_0 \approx 6.7 \cdot 10^{-7}$ Kg/m^2 [18]. We assume $v_c \simeq v_F$ due to gate-induced screening.
[18] M. S. Dresselhaus and P. C. Eklund, Adv. Phys. **49**, 705 (2000).
[19] H. Suzuura and T. Ando, Phys. Rev. B **65**, 235412 (2002).
[20] Here, only the case $\delta \leq 1$ and $y_0 + L_v \leq L_d$ is quoted.
[21] P. Ullersma, Physica **32**, 27 (1966).
[22] F. Cavaliere *et al.*, in preparation.
[23] In these expressions we neglected charge-dependent phase factors, irrelevant for our analysis.
[24] A. De Martino and R. Egger, Phys. Rev. B **67**, 235418

(2003).
[25] K. Bolotin *et al.*, Phys. Rev. Lett. **101**, 096802 (2008).
[26] R. Egger, Phys. Rev. Lett. **83**, 5547 (1999).
[27] D. H. Cobden and J. Nygård, Phys. Rev. Lett. **89**, 046803 (2002).
[28] M. Merlo, F. Haupt, F. Cavaliere, and M. Sassetti, New J. Phys. **10**, 023008 (2008).
[29] For NDC in the coherent regime see e.g. G. Begemann *et al.*, Phys. Rev. B **77**, 201406(R) (2008); M. G. Schultz and F. von Oppen, Phys. Rev. B **80**, 033302 (2009).
[30] C. Seoanez, F. Guinea and A. H. Castro Neto, Appl. Phys. Lett. **78**, 60002 (2007).
[31] M. Ciorga *et al.*, Appl. Phys. Lett. **80**, 2177 (2002).
[32] F. Cavaliere *et al.*, Phys. Rev. Lett. **93**, 036803 (2004).
[33] F. Haupt, F. Cavaliere, R. Fazio, and M. Sassetti, Phys. Rev. B **74**, 205328 (2006).